Macromolecules

Article

pubs.acs.org/Macromolecules

Highly Efficient and Reversible Iodine Capture in Hexaphenylbenzene-Based Conjugated Microporous Polymers

Yaozu Liao,*[,†,‡] Jens Weber,[§] Benjamin M. Mills,[‡] Zihao Ren,[‡] and Charl F. J. Faul*[,‡]

[†]State Key Laboratory for Modification of Chemical Fibers and Polymer Materials & College of Materials Science and Engineering, Donghua University, Shanghai 201620, P. R. China

[‡]School of Chemistry, University of Bristol, Bristol BS8 1TS, U.K.

[§]Department of Chemistry, Hochschule Zittau/Görlitz (University of Applied Science), Theodor-Körner-Allee 16, D-02763 Zittau, Germany

Supporting Information

ABSTRACT: The effective and safe capture and storage of radioactive iodine (^{129}I or ^{131}I) is of significant importance during nuclear waste storage and nuclear energy generation. Here we present detailed evidence of highly efficient and reversible iodine capture in hexaphenylbenzene-based conjugated microporous polymers (HCMPs), synthesized via Buchwald–Hartwig (BH) cross-coupling of a hexakis(4-bromophenyl)benzene (HBB) core and aryl diamine linkers. The HCMPs present moderate surface areas up to 430 $m^2\ g^{-1}$, with narrow pore size distribution and uniform ultramicropore sizes of less than 1 nm. Porous properties are controlled by the strut lengths and rigidities of linkers, while porosity and uptake properties can be tuned by changing the oxidation state of the HCMPs. The presence of a high number of amine functional groups combined with microporosity provides the HCMPs with extremely high iodine affinity with uptake capacities up to 336 wt %, which is to the best of our knowledge the highest reported to date. Two ways to release the adsorbed iodine were explored: either slow release into ethanol or quick release upon heating (with a high degree of control). Spectral studies indicate that the combination of microporosity, amine functionality, and abundant π-electrons ensured well-defined host–guest interactions and controlled uptake of iodine. In addition, the HCMPs could be recycled while maintaining 90% iodine uptake capacity (up to 295%). We envisage wider application of these materials in the facile uptake and removal of unwanted oxidants from the environment.

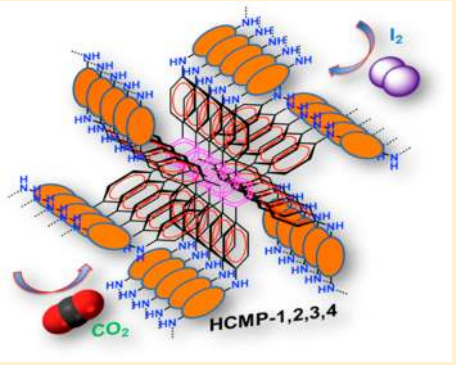

INTRODUCTION

Microporous adsorbents for selective capture of micropollutants have received increasing interest in recent years.[1−4] Capture of volatile iodine (I_2) is of special interest, since the long-lived radioactive iodine isotopes (e.g., ^{129}I or ^{131}I) need to be removed from exhaust fumes of nuclear power plants regularly.[2−4] Additionally, fast removal of radioactive iodine is needed in the case of nuclear accidents, as iodine shows significant biouptake and can be accumulated in living matter. Suitable adsorbents that can tackle this issue of global importance are therefore in high demand. Generally, inorganic composite adsorbents[2,3] such as silver-based zeolites or aerogels are used for radioactive iodine capture. But these silver-containing adsorbents have low uptake capacities, due to their limited accessible surface areas. In particular, the use of materials with high silver content is not attractive because of the high associated cost and adverse environmental impact of the silver. Porous crystalline metal–organic frameworks (MOFs), a new type of adsorbent, have recently been explored for iodine capture.[4] These porous adsorbents have better uptake capacity compared with the silver-based adsorbents. However, the poor water and moisture stabilities of the MOFs impair their iodine capture capability and subsequent safe storage in practical applications, since the exhaust fumes of nuclear power plants contain high levels of water vapor. Therefore, the development of new porous adsorbents with a large surface area, high pore volume, and robust chemical and thermal stability for iodine capture still remains a significant challenge.

The design and synthesis of conjugated microporous polymers (CMPs) with pore sizes of less than 2 nm have generated enormous interest in recent years as potentially suitable candidates for various applications. In addition, these highly unsaturated π-bond-rich materials also have the potential to exhibit additional attractive optoelectronic properties and features. Generally, interest is based on promises of significantly increased performance compared with standard porous materials in applications such as gas separation and storage, energy storage (e.g., capacitors), catalysis, and photovoltaics.[5,6] Specifically, CMPs have been shown to be effective adsorbents

Received: April 30, 2016
Revised: August 26, 2016
Published: September 1, 2016

DOI: 10.1021/acs.macromol.6b00901
Macromolecules 2016, 49, 6322−6333

Scheme 1. Synthetic Route to HCMPs Microporous Adsorbents

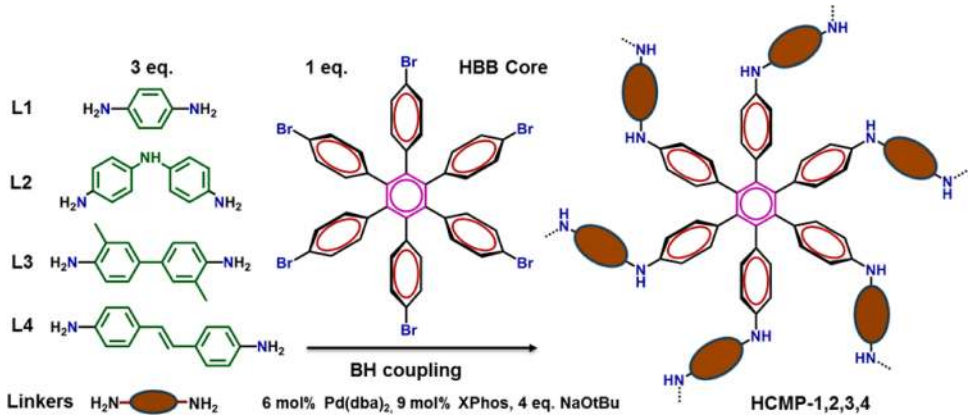

for the greenhouse gas CO_2 and gaseous fuels such as H_2 and CH_4. The presence of light elements (C, H, N, O, and B) makes them less dense than the zeolites and MOFs mentioned above. The vast choice of organic building blocks and diversity of synthetic routes[6] (e.g., Suzuki, Sonogashira−Hagihara and Yamamoto coupling, Schiff-base chemistry, cyclotrimerization, and oxidative polymerization reactions) allow fine-tuning of the specific surface area and porosity of the polymers. The strong covalent bonding and highly unsaturated π-bond-rich nature of the networks afford high thermal and chemical stabilities as well as unique electron-donating characteristics. Previous studies demonstrated that control over a range of properties, including microporosity, surface area, gas uptake, photoluminescence and electrical conductivity, of the CMPs was enabled by altering the strut lengths,[7,8] rigidities,[7,9] contortions,[10−12] and functionalities[13] of the building blocks. For example, spirobifluorene[10,11,14] and bipropylenedioxythiophene[12] as rigid, contorted building blocks have been utilized in the construction of CMPs with strong fluorescence and large specific surface area and high H_2 uptake. Specifically, building blocks based on tetrahedral carbon and silicon centers,[15] cubic siloxane cages,[16] and bulky adamantane moieties[17] have been employed to prepare three-dimensional (3D) porous polymers with high surface area and exceptional gas adsorption properties. However, few examples have been reported where CMPs have been used to address iodine absorption.[18,19]

Hexaphenylbenzene (HPB) is an interesting structural unit for the construction of a range of organic materials because of its rigidity and propeller-like shape generated from the mutual steric interactions of the peripheral phenyl rings (Figure S1). The propeller-like conformation enables π-interactions between the peripheral aryl rings facing each other, and the resulting accumulation of the π-interactions lead to a so-called "toroidal delocalization".[20] HPB derivatives are therefore regarded as promising organic electronic materials with unique 3D topologies.[21] Moreover, HPB possesses a complex molecular architecture that would lead to the imperfect stacking of molecules in the solid state, as shown by numerous crystal structures of its derivatives.[22] This feature, so-called "internal molecular free volume",[23] allows for the easy passage of solvent and reagents as well as for improved gas storage properties.[24] This feature has been exemplified by using HPB as a building block for syntheses of polymers of intrinsic microporosity[22] and certain CMPs.[25−27]

Inspired by these developments, and keen to continue to exploit the BH cross-coupling strategy for CMP production,[7] we here extend the amine-CMP family by the synthesis of novel HPB-based CMPs through the BH cross-coupling of the hexakis(4-bromophenyl)benzene (HBB) core and selected aryl diamine linkers (Scheme 1). This approach, exploiting careful choice of strut lengths and rigidities of the diamine and additional functionalities, would allow formation of 3D amine-linked HPB-based conjugated microporous polymers (HCMPs). It is expected that the resultant HCMP properties (optoelectronics, porosity, and selective gas uptake, for example) will depend largely on the choice of the aryl linkers. Within the present study, we therefore wish to elucidate this relation and explore further design rules related to their unique electronic features to tune such properties. More importantly, to further investigate the adsorption performance, iodine vapor, as a safe analogue to iodine radioisotopes (^{129}I and ^{131}I, found for instance in gaseous nuclear waste), was employed as a guest molecule for micropollutant capture measurements. Controlled release of iodine and recyclability of the adsorbents were also investigated, aiming to provide an appropriate approach to facile nuclear waste management.

RESULTS AND DISCUSSION

Synthesis, Structure, and Morphology of HCMPs. The HCMPs were synthesized using a palladium-catalyzed BH cross-coupling reaction.[28] After work-up and purification, the products (**HCMP-1**, **-2**, **-3**, and **-4** with different aryl diamine linkers **L1**, **L2**, **L3**, and **L4**) were obtained as brown, dark-blue, yellow, and dark-brown solids (Figure S2), with yields of 95, 78, 90, and 81%, respectively. The brown products likely contain oxidized materials that provide opportunities for charge-transfer (CT) interactions with reduced materials. The dark blue products may be indicative of a cationic material, similar to Würster's blue.[29] This is especially expected for the polymers that contain the phenylenediamine structure. After treatment with 1.0 M anhydrous hydrazine/tetrahydrofuran in a glovebox, **HCMP-1** and **-2** became gray while the **HCMP-3** and **-4** showed no obvious changes in color. This behavior indicated that the pristine **HCMP-1** and **-2** containing the π-electron-rich phenylenediamine group were sensitive to exposure to the reducing hydrazine. All the products were insoluble in a range of organic solvents, including dimethyl sulfoxide (DMSO), *N*-methyl-2-pyrrolidone (NMP), dimethylformamide (DMF), chloroform ($CHCl_3$), tetrahydrofuran (THF), and ethanol (EtOH), hinting at a high degree of cross-linking.

The successful preparation of HCMP networks was confirmed by solid-state ultraviolet−visible−near-infrared

DOI: 10.1021/acs.macromol.6b00901
Macromolecules 2016, 49, 6322−6333

(UV−vis/NIR), Fourier-transform infrared (FT-IR), and solid-state ^{13}C cross-polarization magic angle spinning nuclear magnetic resonance (CP/MAS NMR) spectroscopies and powder X-ray diffraction (XRD). The UV−vis/NIR spectra of fully conjugated **HCMP-1**, **-2**, and **-3** exhibited two peaks at 286−328 and 485−755 nm, typically attributed to $\pi-\pi^*$ transitions of benzenoid (B) and quinoid (Q) groups (Figure 1).[28] **HCMP-4** displayed a broad peak at 966 nm; although it

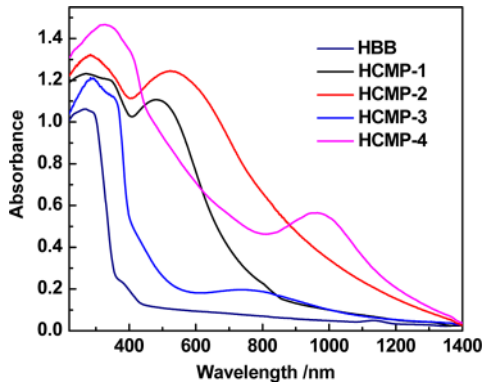

Figure 1. Solid-state UV−vis/NIR spectra of HBB and HCMPs.

has not been possible to assign the origin of the peak unambiguously, we tentatively assign this long-wavelength feature to the presence of radical cation species in the formed network (see calculations and discussions below). It is noteworthy that the second peaks observed in **HCMP-1**, **-2**, **-3**, and **-4** bathochromically shifted from 485 to 528, to 755, and to 966 nm, respectively, most probably owing to a combination of the increased strut lengths of the diamine linkers and the presence of mixed oxidation states within the network structures.

FT-IR spectra showed that the primary aryl amine (−Ph−NH_2) of the linkers became B-type secondary amine (−Ph−NH−) moieties in the HCMPs, since their corresponding bending vibrational bands hypsochromically shifted from 1635 to 1605 cm^{-1}, and the stretching vibrational bands of C−N bathochromically shifted from 1259 to 1300 cm^{-1} (Figure 2).

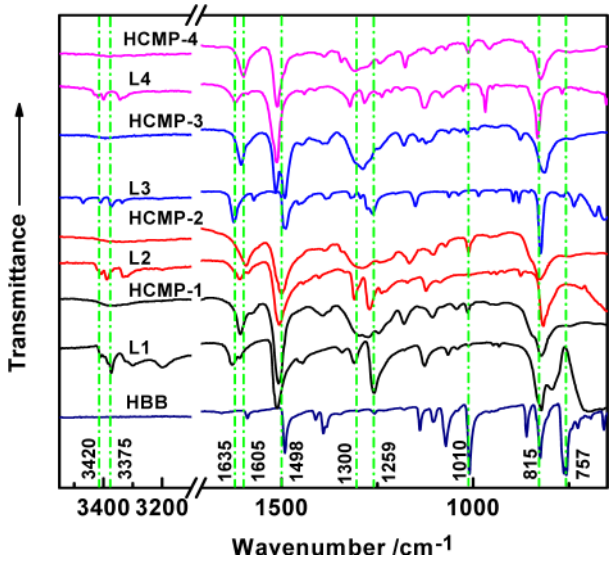

Figure 2. FT-IR spectra of HBB, linkers, and HCMPs.

The bands at 3375 and 3420 cm^{-1} (due to the symmetrical stretching of primary amines) and the bands at 757 and 1010 cm^{-1} (due to the aryl C−Br stretching vibrations[30,31]) almost disappeared in the produced HCMPs. The bending bands at 1498 and 815 cm^{-1} assigned to Q-type imine bonds (−N═C−) and −CH− of substituted benzene, respectively, were present in the spectra of the products, indicating the success of our BH cross-coupling approach.

All the HCMPs showed two resonances at ∼140.5 and 132.5 ppm in their ^{13}C CP/MAS NMR spectra (Figure 3), owing to the substituted phenyl carbon atoms connected with nitrogen (a) and carbon (b) atoms. Two further resonances were observed at ∼127.1 and 117.2 ppm owing to the unsubstituted phenyl carbon atoms (c and d), respectively. Note that additional resonances (e) at 17.5 and 115.1 ppm could be attributed to the methyl and alkenyl groups of **HCMP-3** and **HCMP-4**, respectively. Furthermore, an additional peak at 157.9 ppm (asterisk) was observed in both **HCMP-1** and **HCMP-2** but was absent in both **HCMP-3** and **HCMP-4**. The structures of **HCMP-1** and **HCMP-2** are comparable with the conventional conjugated polymer, polyaniline (PANi). Previous studies suggested that the peak around 157.3 ppm is normally attributed to the C═N quinoid resonance, since phenylene-diamine and diaminodiphenylamine units are easily oxidized in air.[32] The NMR results further confirmed the formation of the expected conjugated polymer networks.

Powder XRD measurements revealed that all four polymer networks were amorphous in nature, as found for other HPB-based networks (Figure S3).[26] Scanning electron microscope (SEM) images showed that the **HCMP-1** and **HCMP-3** networks were composed of aggregated nanoparticles with diameters of 200−500 nm (Figure 4), similar to those observed in HPB-triptycene-based CMPs.[26,33] The morphologies of **HCMP-2** and **HCMP-4** networks exhibited aggregated and intergrown polydisperse particles with sizes ranging from hundreds of nanometers to micrometers. Careful high-resolution transmission electron microscopy (TEM) investigations of the HCMP networks showed the primary microporous particles with black nanoparticles with diameters of 3−5 nm incorporated (Figure 5). TEM/energy dispersive X-ray (EDX) analyses showed that the nanoparticles mainly consist of palladium (Pd) uniformly dispersed in the polymer networks (Figure S4). As determined by elemental analyses, the Pd residues were found to be 0.78−1.73 wt % in the HCMPs. It is expected that the Pd would interact with the amine groups present in high concentration. At the same time, our TEM investigations seem to indicate that the Pd residues were formed *in situ*, and their presence was limited within the micropores generated by the polymer networks (and thus explaining why, even after extensive purification, the catalyst residues could not be removed). However, the presence of Pd residues make these polymer networks potentially promising for exploring nanoparticle-based catalysis in the future.

Thermal Stability, Surface Area and Porosities of HCMPs. The thermogravimetric analysis (TGA) of HCMPs under N_2 (Figure S5) showed that these materials were stable up to 500 °C and yielded >70 wt % chars when heated to 1000 °C. The excellent thermal stability of the HCMPs is attributed to their rigid and highly cross-linked network structures resulting from the formation of multiple stable C−N bonds.

Nitrogen adsorption/desorption isotherms of HCMPs measured at 77.4 K are shown in Figure 6. **HCMP-1** showed the highest porosity (S_{BET} = 430 m^2 g^{-1}) and N_2 uptake.

DOI: 10.1021/acs.macromol.6b00901
Macromolecules 2016, 49, 6322−6333

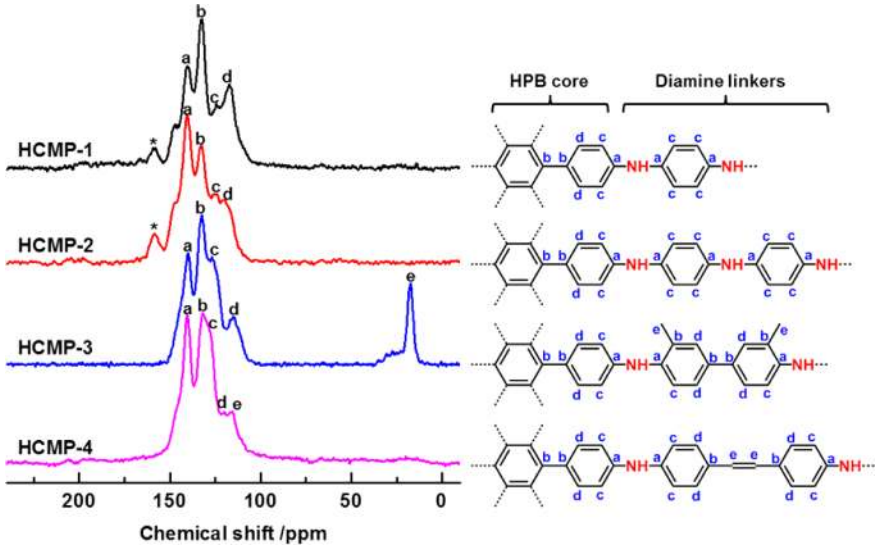

Figure 3. Solid-state ^{13}C CP/MAS NMR spectra of HCMPs (asterisks mark C═N bands).

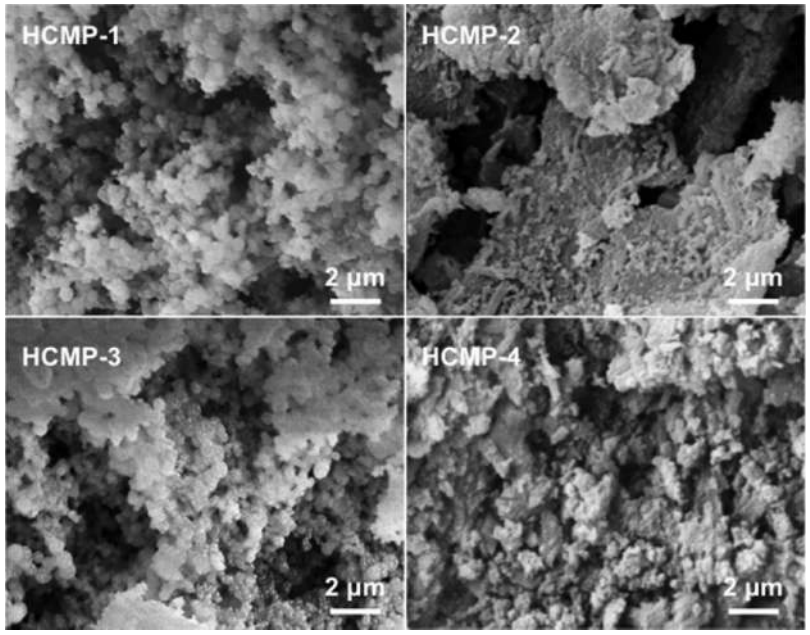

Figure 4. SEM images of HCMPs.

HCMP-1 and **-2** showed a significant low-pressure hysteresis, which is commonly found for polymeric materials with very small micropores that can only be accessed with some restrictions.[34] For **HCMP-3** and **-4**, no signs of microporosity were found from the nitrogen adsorption data. These results indicate that only short and rigid linkers such as **L1** lead to pronounced microporosity under the reactions conditions used. This finding is in contrast to what has been found in previous PTPA networks,[7] created by a similar synthetic protocol. There, shorter linkers (e.g., **L1**) gave lower surface areas, whereas longer linkers (e.g., **L4**) resulted in higher surface areas. Nitrogen adsorption/desorption studies also indicated the presence of some outer surface area (increased uptake at $p/p_0 > 0.95$). This finding is in accordance with electron microscopy results that showed the presence of small primary particles.

The drawbacks of N_2 adsorption at 77.4 K for the characterization of microporous polymers are well-known, and CO_2 adsorption at 273.15 K is an accepted additional tool.[35] Hence, CO_2 adsorption at 273.15 K was measured for all HCMP materials (see Figure 7a) to gain more information on the microporosity and provide an initial indication of their potential as conjugated microporous adsorbents. Table 1 summarizes the results obtained from gas adsorption studies. All materials showed a moderate CO_2 uptake. In line with the results of the N_2 experiments at 77.4 K, the highest porosity was found for **HCMP-1**, followed by **HCMP-2**, **-3**, and **-4**. The CO_2 uptake at 273.15 K and 1 bar were in the range of 1−1.7 mmol g^{-1}, which is a commonly found range for microporous polymers (see Figure S6). The isotherms showed almost no hysteresis (hence no obvious kinetic restrictions for CO_2 sorption) and were analyzed using the commercialized grand canonical Monte Carlo (GCMC) methodology to extract porosity information (see Table 1). The microporosity as probed by CO_2 was found to be comparable to results obtained

DOI: 10.1021/acs.macromol.6b00901
Macromolecules 2016, 49, 6322−6333

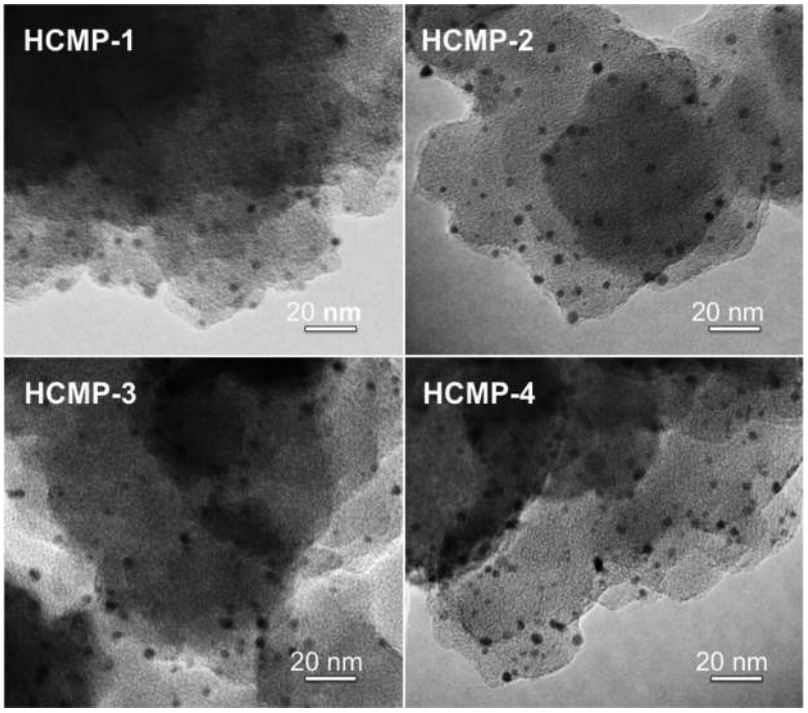

Figure 5. High-resolution TEM images of HCMPs.

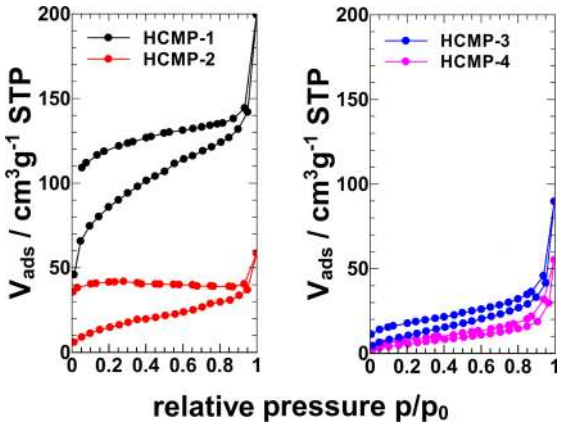

Figure 6. Nitrogen adsorption/desorption isotherms of (left) **HCMP-1** and **-2** and (right) **HCMP-3** and **-4** (77.4 K).

from N_2 at 77.4 K for **HCMP-1**. All other materials showed a higher microporosity when analyzed by CO_2, indicating that not all or no pores could be accessed by N_2 (77.4 K, see Table 1 for details).

The shape of the pore size distributions (PSDs) obtained seems to be similar for all HCMPs with the majority of pores with sizes <1 nm (Figure 7b). Interestingly, **HCMP-3** seems to have slightly smaller pores compared to **HCMP-2** (also evidenced by the crossing isotherms, Figure 7a).[36] The effect is however small, and the slightly different intermolecular interactions (see discussion below) might interfere with the pore size analysis. Generally, the PSDs show that all polymers have pores of various sizes. With regard to the monomer geometry, it can once more be concluded that longer strut monomers (e.g., **L4**) led to slightly lowered porosity. The presence of fairly small pores in combination with a uniform distribution of polar amine moieties is expected to result in favorable interactions between some adsorbate molecules and the microporous adsorbent network.[37] On the basis of the CO_2 adsorption isotherms measured at 303.15 K (Figure S7), the ideal adsorbed solution theory (IAST) selectivity of CO_2 over N_2 was calculated to be as high as 105 for **HCMP-1** and 45 for **HCMP-2** at ambient conditions (1.0 bar, 303.15 K) (Figures S8 and S9). The CO_2 uptake capacities and selectivities are comparable, if not slightly better, to the values obtained by previously reported CMPs (Table S1). Note that upon reduction by anhydrous hydrazine, the N_2 adsorption capacity of **HCMP-1** and **HCMP-3** increased, and the corresponding specific surface area increased from 308 to 410 m^2/g and 50 to 92 m^2/g (based on adsorption isotherms, Figure S10a), respectively. However, the CO_2 adsorption capacities of reduced **HCMP-1** and **HCMP-3** dramatically decreased from 7.5 to 3.9% and 5.1 to 3.2% (Figure S10b), respectively. Interestingly, although the CO_2 uptake capacity decreased, the surface area of networks increased with an increased number of reduced −NH− units after treatment with hydrazine. This phenomenon provided us with the ability to carefully control the CO_2 uptake in a facile fashion by simply adjusting the oxidation state of the polymer networks. We found, for example, that the CO_2 adsorption capacity of **HCMP-1** could be remarkably enhanced to 10.3 wt % after oxidation by H_2O_2. However, the real area of interest for these conjugated microporous adsorbent materials was found for their iodine uptake behavior.

Iodine Capture and Adsorption by HCMPs. Electron-rich aromatic networks with conjugated π-electrons provide a number of possibilities to interact with iodine, thereby providing a possible route to increase the amount of iodine adsorbed.[38] It was therefore expected that through a combination of attractive electronic properties and the advantages of porosity and remarkable stability, the as-synthesized HCMP samples would be promising candidates for iodine capture. Upon exposure to iodine vapor at 358.15 K and 1.0 bar, the as-synthesized samples became gradually darker

DOI: 10.1021/acs.macromol.6b00901
Macromolecules 2016, 49, 6322−6333

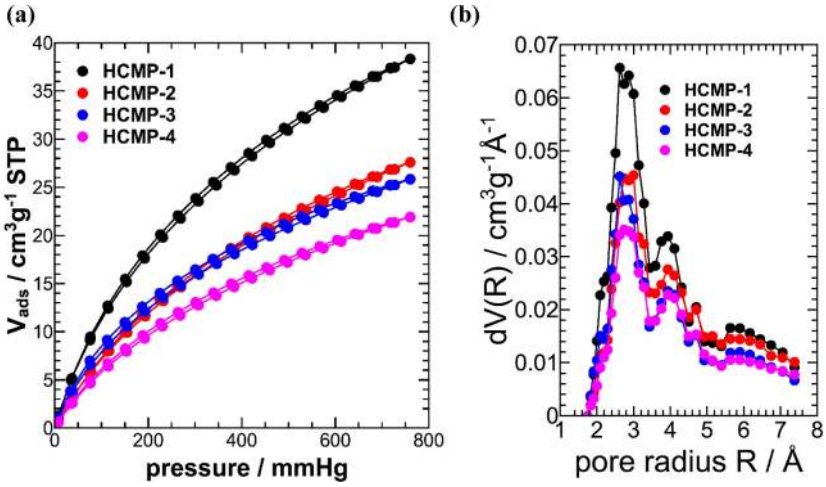

Figure 7. (a) CO_2 adsorption/desorption isotherm at 273 K and (b) PSDs of HCMPs obtained from GCMC analysis of the CO_2 adsorption data.

Table 1. Porosity Parameters and CO_2 Uptake of the Microporous HCMPs at 1 bar

						CO_2 uptake (wt %)	
HCMP	S_{BET}[a,b] (m^2 g^{-1})	PV[c] (cm^3 g^{-1})	MPV[d] (cm^3 g^{-1})	μ-pore S_{GCMC}[e] (m^2 g^{-1})	MPV_{GCMC}[e] (cm^3 g^{-1})	273 K	303 K
1	308/430	0.22	0.18	393	0.14	7.5	3.8
2	58/153	0.06	0.06	259	0.11	5.4	2.5
3	50/82	0.08	n.a.	267	0.10	5.1	n.d.
4	28/n.a.	n.a.	n.a.	233	0.08	4.3	n.d.

[a]Surface area calculated from N_2 adsorption isotherms using the BET equation. [b]Surface area calculated from the desorption branch of the N_2 isotherms using the BET equation. [c]Pore volume calculated from nitrogen uptake at $p/p_0 = 0.95$. [d]Micropore volume calculated from QSDFT (slit pore model, desorption branch) analysis of N_2 data. [e]Micropore surface area determined from GCMC analysis of the CO_2 adsorption data at 273 K. n.a. = not applicable; n.d. = not determined.

as iodine diffused into them. For example, yellow **HCMP-3** instantly became brown upon exposure to iodine, gradually darkening until becoming black throughout (Figure S11). The iodine-loaded adsorbents were weighed regularly at ambient conditions; equilibrium uptake for all the HCMPs was reached quickly within 30−45 min (Figure 8). This sorption behavior was much faster than that observed in most porous iodine adsorbents (see detailed comparisons in Table S2).

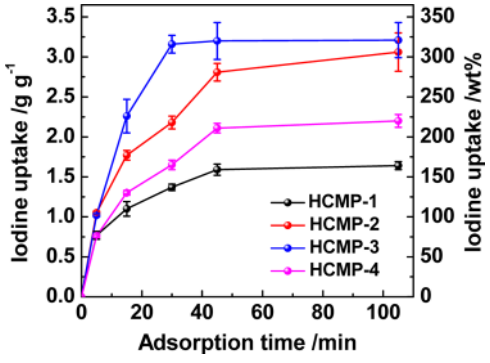

Figure 8. Gravimetric changes of iodine uptake capacity of HCMPs as a function of time at 358.15 K and ambient pressure.

However, the iodine uptake capacity of HCMPs does not simply correlate to the surface areas or pore volumes of the HCMPs as determined by gas adsorption/desorption; this behavior is similar to that found for MOFs,[39] porous polymers,[14] and other porous adsorbents such as aerogels[3] and coals.[40] For example, **HCMP-3**, with the third highest S_{BET} (82 m^2 g^{-1}), exhibited the highest equilibrium uptake capacity of iodine (C_u) of up to 316 wt % (3.16 g g^{-1}), a value that is to the best of our knowledge, the highest reported to date. The adsorbed amount would correspond to a volume of 0.6 cm^3 g^{-1} for **HCMP-3**, which is much larger than the actual pore volume (0.08 cm^3 g^{-1}). Even for **HCMP-1** a mismatch between 0.3 cm^3 g^{-1} (iodine uptake) and a pore volume of 0.22 cm^3 g^{-1} exists. Such strong mismatches are well-known from the interaction of iodine and "soft" coals (i.e., coals that can swell significantly) and is attributed to a combination of strong interactions and swelling or expansion of the adsorbent.[40] In other words, the porosity is not stable enough to be probed in the dry state (i.e., where pores collapsed or closed due to the action of interfacial energy). Such behavior is well-known for CMPs as discussed previously.[34] However, pores can reopen if the energy gain from association between the HCMPs and iodine is high enough to counteract forces leading to closure and can explain the mismatch observed here.

Analysis of the kinetic data by a pseudo-second-order kinetic model supports the assumption of strong interaction (Figure S12 and Table S3). The data can be well described by such a model (but not by a first-order model), which is especially effective if chemisorption-type processes occur.[41] Interestingly, the kinetic data do however show that the rate constant for adsorption in **HCMP-1** is highest; i.e., the open porosity enables a fast filling of the adsorbent. However, total uptake in **HCMP-1** is the lowest of the materials prepared here, indicative of the rigidity originating from the short linker used. On the contrary, the other HCMPs with longer linkers fill more slowly, an effect that might be related to the necessary expansion/

DOI: 10.1021/acs.macromol.6b00901
Macromolecules 2016, 49, 6322−6333

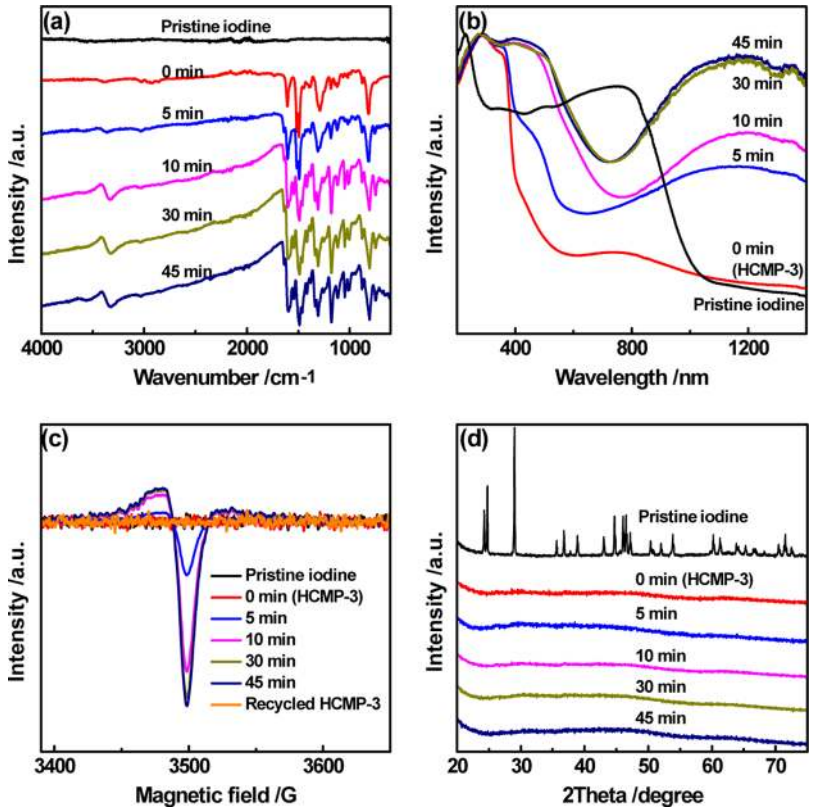

Figure 9. (a) FT-IR, (b) UV−vis/NIR, (c) ESR, and (d) XRD spectra of pristine iodine, **HCMP-3**, and iodine-loaded **HCMP-3** with different times of iodine vapor exposure. Note that an ESR spectrum of recycled **HCMP-3** is also shown in (c).

rearrangement of the adsorbent in order to accommodate the iodine.

Fortunately, the strong interactions expected to exist between the π-electron systems and iodine in the conjugated microporous adsorbents could be preliminarily studied using FT-IR, UV−vis/NIR, electron spin resonance (ESR), XRD, and X-ray photoelectron spectroscopy (XPS) analyses. Here we focus our discussions on **HCMP-3**, with the other materials showing similar trends. When the FT-IR spectra of parent and iodine-loaded networks were compared, it was found that the iodine-loaded **HCMP-3** exhibited considerably enhanced N−H stretching vibrations (3325−3400 cm^{-1}, Figure 9a). The center of the peak shifted from 3365 to 3325 cm^{-1} with increasing iodine uptake time, indicating noncovalent interactions between amine groups of **HCMP-3** with iodine.[42] The B, Q, and CH bands of **HCMP-3** at 1605, 1498, and 815 cm^{-1} shifted to 1595, 1488, and 805 cm^{-1}, respectively, while the corresponding C−N bands shifted from 1286 to 1310 cm^{-1} (see Figure S13 for more details). Indications are that iodine adsorption could occur at N−H and C−N units as well as aromatic rings in the **HCMP-3** molecular chains, which is similar to the phenomenon observed in iodine-doped PANi.[43] This is most likely due to the formation of a charge transfer (CT) complex between **HCMP-3** and polyiodide anions, as indicated by a similar case of iodine-loaded porous conjugated organic cages.[44] The resulting CT interactions with the benzene rings are sufficient to cause these band-shift effects. These interactions are confirmed in the following experimental observations and discussions. The UV−vis/NIR spectra of all iodine-loaded **HCMP-3** samples (Figure 9b) showed broad absorption features from 1000 to >1400 nm attributed to polarons. A polaron band is commonly observed in iodine-doped polyacetylene or acid-doped PANi.[45] Importantly, no additional peaks at ~800 nm resulting from pristine iodine crystals were observed in any of the iodine-loaded sorbents, indicating that the adsorbed iodine molecules were completely transformed into polyiodide anions.

Evidence for the existence of CT interactions in the iodine-loaded HCMPs was furthermore provided by ESR, XRD, and XPS analyses. There were no paramagnetic signals in pristine iodine and HCMPs at room temperature (Figure S14). In contrast, obvious signals were observed in the iodine-loaded HCMPs, with the highest intensity observed for iodine-loaded **HCMP-3**. It is observed that the paramagnetic signal intensity of **HCMP-3** drastically increased with prolonged exposure to iodine, reaching equilibrium after 30 min (Figure 9c), which corresponds to the maximum gravimetric uptake of iodine as shown in Figure 8. Upon heating the iodine-loaded **HCMP-3** at 398.15 K for 1 h, the paramagnetic signals completely disappeared when measured at room temperature. Although iodine readily forms CT complexes with aromatic π-conjugated systems,[46] the paramagnetic signals of the iodine species in these complexes are usually not observed at room temperature because of their large anisotropy and rapid electron-spin relaxation.[47] The presence and disappearance of the paramagnetic signals can therefore be safely assigned to polymeric cation radicals as a result of the CT interactions between HCMPs and iodine. Moreover, powder XRD measurements (Figure 9d) revealed that iodine-loaded **HCMP-3** was amorphous in nature without any prominent crystalline diffraction peaks, even when the iodine loading was as high as 316 wt %. The $I_{3d_{5/2}}$ XPS spectrum of iodine-loaded **HCMP-3** showed two peaks at 618.57 and 619.89 eV (Figure S15),

DOI: 10.1021/acs.macromol.6b00901
Macromolecules 2016, 49, 6322−6333

which were attributed to the I_3^- and I_5^- anions, respectively.[48] This revealed that the iodine was chemically adsorbed on the surface of **HCMP-3** as a polyiodide in an ionic state. Such chemisorptive processes are in accordance with the pseudo-second-order adsorption kinetics described above. As equilibrium uptake was achieved after 30 min of exposure and adsorption (see Figure 8), all spectrometric analyses of iodine-loaded **HCMP-3** indicated no obvious further spectral changes. We conclude that the microporosity and the presence of amine moieties, combined with abundant π-electrons, produced well-defined host−guest interactions for very high uptake of iodine.

On the basis of the data presented above, we believe that chemical interaction between HCMPs and iodine is mainly responsible for the high iodine uptake capacities (150−320 wt %). After reducing the polymers, we found that the iodine uptake capacities of iodine (358.15 K, 1.0 bar, and 45 min) could be further increased from 159 to 291 wt % and 316 to 336 wt %, respectively. This increase can most probably be ascribed to the increased number of amine groups produced by reduction, resulting in stronger CT interactions with the oxidizing iodine. In addition, the small pores (even the closed pores that are not accessible by gas adsorption but that can potentially be opened by the adsorption of iodine with significant energy gain) within the HCMPs can enhance the uptake.[19,41,49]

In an attempt to further identify the reasons for the differences in the iodine uptake capacity and UV−vis/NIR spectra of the different HCMPs, we explored the use of time-dependent density functional theory (TD-DFT) calculations to provide additional insight. This method has only very rarely been applied to CMPs.[50] To model HCMPs, we used fragments of the networks consisting of two hexaphenylbenzene groups joined by the appropriate diamine linkers **L1**, **L2**, **L3**, and **L4** (Table S4). The structures of the model fragments were first minimized by DFT in Gaussian 09 using the B3LYP functional and the 6-31G* basis set,[51] with the spectra then calculated in a separate TD-DFT step with the CAM-B3LYP functional.[52] We found similar trends in the experimental and calculated spectra, such as the progression to longer wavelength maxima in the order **HCMP-1** < **HCMP-2** < **HCMP-3** < **HCMP-4** for the oxidized networks and a very similar trend for the reduced networks: **HCMP-1** < **HCMP-2** ≈ **HCMP-3** < **HCMP-4** (Figures S16 and S17 and Table S5). For the doped cation radical models, the found order is **HCMP-1** < **HCMP-2** < **HCMP-4** < **HCMP-3** (Figures S18 and S19 and Table S6). The experimental UV−vis/NIR spectrum of **HCMP-3** also shows an absorption band at longer wavelengths than the other HCMPs. These initial results therefore provide support that **HCMP-3**'s anomalously high iodine uptake originated from its electronic structure. However, there was no close match between experimental and theoretical UV−vis/NIR spectra, and the calculated HOMO and ionization energies of the HCMPs (as two possibilities to evaluate and compare differences of the starting HCMPs) did not correlate with their iodine uptakes, either. It is therefore not possible to draw firm and detailed conclusions concerning the chemistry and physical properties of HCMPs from these models. We suggest that larger and more complicated network fragments (also allowing for interactions between neighboring linkers and between the networks and iodide or polyiodide counterions) would need to be modeled to achieve closer agreement to the obtained experimental results. Alternatively, larger basis sets may lead to calculated energies in closer agreement with the experimental findings, albeit at significantly higher computational cost as the fragments modeled are large.

Additionally, such iodine uptake could be expected to yield changes in conductivity for HCMPs as compared to other conjugated polymers/oligomers.[53] Preliminary testing showed that the insulating **HCMP-3** (in pellet form) became electrically conducting as its sheet resistance decreased from >100 MΩ/square to 230 KΩ/square after uptake of iodine at 358.15 K for 30 min. Additional studies are now being conducted in our laboratories to exploit this behavior in more application-driven areas.

Iodine Release and Recyclability of the HCMP Adsorbents. Iodine release occurred if the iodine-loaded samples were placed in organic solvents such as ethanol at room temperature. Information on the release kinetics was obtained by time-dependent *in situ* measurements of the UV−vis absorbance of the iodine-containing ethanol. The UV−vis spectra of all extracts showed two absorbance maxima at 291 and 360 nm, assigned to polyiodide anions (Figure S20).[4,54] The amount of iodine released from all the HCMPs adsorbents increased linearly with time, following pseudo-zero-order kinetics within the monitored time frame (70 min), which cannot be compared directly to the vapor adsorption/desorption experiments. We believe that this release behavior is governed by host−guest interactions,[19] facilitating the regeneration of the adsorbent for reuse. The speed of iodine release (estimated based on the slope of linear plots, Figure 10; see detailed comparison in Table S7) follows the order **HCMP-4** (0.013) > **HCMP-2** (0.009) = **HCMP-1** (0.009) > **HCMP-3** (0.004). Strong π-electron−iodine host−guest interactions would facilitate iodine capture, while it would also impair the dissociation of iodine from the adsorbents, resulting in the lowest release speed observed in the **HCMP-3** system.

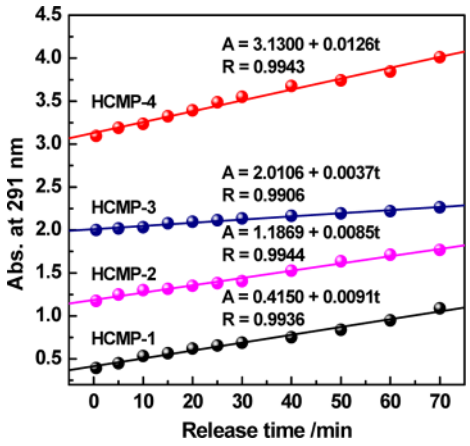

Figure 10. Controlled release rate of iodine in **HCMP-1**, **-2**, **-3** and **-4** in the first 70 min determined by UV−vis absorbance at 291 nm. *A* = absorbance; *R* = linear correlation coefficient.

Other studies showed that iodine release (and adsorbent material recovery for recycling) could also be induced by heating iodine-loaded samples at 393−473 K.[2−4,42] When the iodine-loaded **HCMP-3** was heated in air at 398.15 K and 1.0 bar for 30 min, iodine release efficiency (E_r) was as high as 98.8% (Figure 11). Interestingly, the thermal desorption follows pseudo-second-order kinetics as well, indicating that adsorption/desorption observed for all the gas phase studies follows a comparable mechanism.

DOI: 10.1021/acs.macromol.6b00901
Macromolecules 2016, 49, 6322−6333

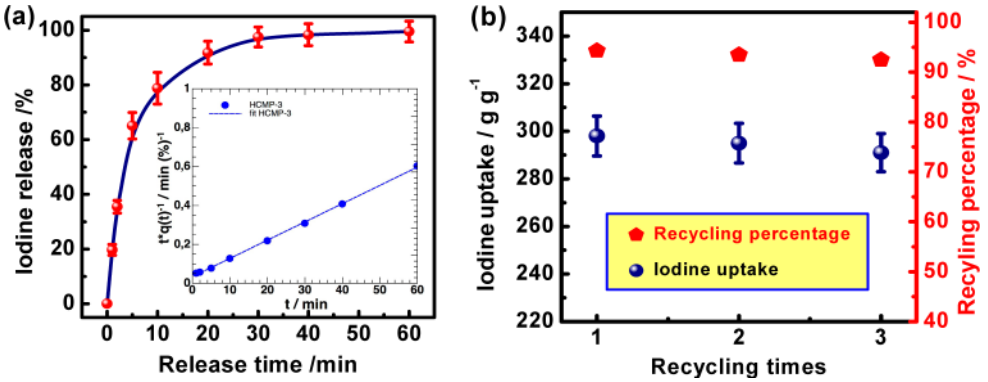

Figure 11. (a) Controlled release of iodine upon heating the loaded-**HCMP-3** at 398.15 K. Inset figure shows kinetic data, pseudo-second-order rate law. (b) Recycling percentage of **HCMP-3** (recycling parameters: 1.0 bar, 398.15 K, and 60 min).

The excellent iodine release encouraged us to exploit the recyclability of the adsorbents. Recycling was performed by taking iodine-loaded **HCMP-3** samples (after exposure of as-synthesized **HCMP-3** to iodine for 30 min at 358.15 K) and heating at 398.15 K for 60 min. These samples were then reused for iodine uptake (358.15 K and 30 min). The iodine uptake capacity (C_u) and recycling percentage (R_p) of recovered **HCMP-3** were found to be 294.8 g g^{-1} upon completion of the first cycle, thus retaining 93.3% of the initial capacity. After a further two cycles (i.e., reused three times), the **HCMP-3** still maintained very high C_u values of 288.5 g g^{-1}, retaining 91.3% of its initial capacity. These very high values make our adsorbents attractive materials for use as robust recyclable and reversible iodine uptake adsorbents.

CONCLUSIONS

A series of hexaphenylbenzene-based conjugated microporous polymers (HCMPs) with secondary amine functionalities have been successfully synthesized from the palladium-catalyzed BH cross-coupling of a hexakis(4-bromophenyl)benzene core and selected aryl diamine linkers (struts). The physical properties of these porous HCMPs, including specific surface area, pore size, and general sorbent properties, could be tuned to some extent by varying the strut lengths and, more importantly, by addressing the redox state of the materials. The HCMPs showed moderate micropore surface areas up to 430 m^2 g^{-1}, narrow pore size distribution with uniform ultramicropore size of less than 1 nm, and moderate CO_2 uptake capability (tunable up to 10 wt %). The HCMPs featured excellent iodine affinity with uptake capacities up to 316 wt %, with further increased uptake possible to 336 wt % after reducing the polymers using anhydrous hydrazine. We suggest that the strong chemical interactions between iodine and the HCMPs can reopen some microporosity/free volume of the polymers (based on the energy gain), which was not accessible to common gas adsorption. These results demonstrate once more the versatility of carefully designed porous materials for wide application. The sublimed iodine molecules could be either slowly delivered to ethanol or quickly released upon heating with a very high degree of control. The HCMP adsorbents could furthermore be recycled with minimal (<10%) loss of iodine uptake capacity. Our results demonstrate that judicious design of CMPs with suitable porosity, intrinsic functionality, and electron-donating properties could find useful application in the capture of greenhouse and harmful volatile gases (including Br_2 and Cl_2) in a wide range of scenarios. However, the development of new theoretical approaches, and the use of appropriate model compounds to ensure efficient computational approaches, is crucial for future materials design. Expanding the scope of gases investigated, and additional testing to ascertain the stability of our materials when exposed to harsh environments (including their tolerance toward radiation damage), are further priority topics for future investigations.

EXPERIMENTAL SECTION

Chemicals. Hexaphenylbenzene (HPB, 98%), *p*-phenylenediamine (99%), *o*-tolidine (97%), 4,4′-diaminostilbene (95%), 4,4′-diaminodiphenylamine (95%), bis(dibenzylideneacetone)palladium(0) (Pd(dba)$_2$, 16.6−20.4% Pd), 2-dicyclohexylphosphino-2′,4′,6′-triisopropylbiphenyl (XPhos, 97%), sodium *tert*-butoxide (NaOtBu, 97%), bromine (99.5%), iodine solids (≥99.8%), and all the solvents with A.R and C.R. grades were purchased from Sigma-Aldrich. 4,4′-Diaminodiphenylamine (97%) was purchased from Tokyo Chemical Industry UK Ltd.

Synthesis of Hexakis(4-bromophenyl)benzene (HBB). HBB was obtained by a modified synthesis procedure.[55] A 100 mL mortar was charged with 2 g of HPB powder, and then 20 mL of bromine was added in six batches over a half hour. The mixture was ground, and reaction started immediately as judged by an evolution of gaseous hydrobromic acid. (*Caution: bromine and hydrobromic acid are highly corrosive and toxic. The reaction must be conducted in keeping with the appropriate safety measures.*) After the addition of bromine was complete, the dark orange slurry was ground for an additional 10 min. The resulting bromine slurry was carefully poured into prechilled ethanol (approximately 195 K, 500 mL). The resulting precipitate was filtered and washed with ethanol (100 mL), aqueous sodium bisulfite (5%, 100 mL), and ethanol (3 × 100 mL). After being dried 72 h under vacuum, 3.5 g (95% yield) of HBB was obtained. ^{1}H NMR (400 MHz, THF-d_8, 25 °C): δ = 7.11 (d, 12H), 6.73 (d, 12H) ppm. IR (neat): 1589, 1491, 1391, 1139, 1071, 1010, 861, 815, 757, 659 cm^{-1}. Anal. Calcd for $C_{42}H_{24}Br_6$: C, 50.04; H, 2.40; Br, 47.56. Found: C, 50.73; H, 2.88; Br, 46.91.

Synthesis of HCMP-1, -2, -3, and -4. A Schlenk tube was charged with HBB (0.25 mmol, 1 equiv), diamine (0.75 mmol, 3 equiv, *p*-phenylenediamine **L1**, 4,4′-diaminodiphenylamine **L2**, *o*-tolidine **L3**, or 4,4′-diaminostilbene **L4**), Pd(dba)$_2$ (17.3 mg, 0.03 mmol, 12 mol %), XPhos (21.5 mg, 0.045 mmol, 18 mol %), and NaOtBu (192.2 mg, 2 mmol, 8 equiv) and placed under a nitrogen atmosphere. Anhydrous toluene (50 mL) was added, and the reaction mixture was heated under stirring to 110 °C. After 24 h, the reaction was cooled to room temperature and products separated by centrifugation. The remaining solids were washed by chloroform, hot deionized water (65 °C), and methanol (3 × 200 mL) and then dried 72 h in a vacuum oven to yield the corresponding amine-linked networks as brown, dark-blue, yellow, and dark-brown powders (see Figure S2) with yields of 78−95%, respectively.

DOI: 10.1021/acs.macromol.6b00901
Macromolecules 2016, 49, 6322−6333

Reduction and Reoxidization of HCMPs. The pristine HCMPs would be oxidized in the air because of their electron-rich characteristics. The as-prepared HCMPs were reduced in order to investigate the surface area, N_2, CO_2, and I_2 adsorption properties of HCMPs in the fully reduced state. Typically, 150 mg of **HCMP-1** was dispersed and treated by 30 mL of anhydrous hydrazine in THF (1.0 mol/L) for 24 h in a glovebox. (*Caution: anhydrous hydrazine is highly toxic and dangerous.*) The reduced **HCMP-1** was then collected by filtration under argon. The samples were degassed at 150 °C for 20 h and kept under N_2 before gas adsorption measurements. 100 mg of reduced **HCMP-1** was added to 50 mL of 30% H_2O_2, sonicated for 30 min, and then stirred 2 h to afford reoxidized **HCMP-1**.

Chemical Structure and Morphology Characterization. Both solid-state ultraviolet visible near-infrared (UV−vis/NIR) and UV−vis spectra were recorded on a Shimadzu UV-2600 spectrometer. Fourier transform infrared (FT-IR) spectra were taken on a PerkinElmer Spectrum 100 spectrometer. Powder X-ray diffraction (XRD) patterns were obtained on a Bruker D8 Advance diffractometer (40 kV, 30 Ma) using Cu Kα radiation (2θ = 5°−75°). Proton nuclear magnetic resonance (^{1}H NMR) spectra were recorded on a Jeol Eclipse-400 (400 MHz) using THF-d_8 as solvent. Solid-state ^{13}C cross-polarization magic angle spinning nuclear magnetic resonance (CP/MAS NMR) spectra were recorded at the Solid State NMR Service, Durham University, on a Varian VNMRS-600 spectrometer using a spin rate of 6800 Hz. Electron spin resonance (ESR) measurements were conducted at room temperature on a Benchtop Micro-ESR ESR spectrometer using a thin-walled capillary tube (2 mm o.d.) loading with 2 cm length of sample powders (scan mode: microwave power of 40 mW, 3000−4000 G, four scans). X-ray photoelectron spectra (XPS) were obtained on a PHI5000 1 Versaprobe-II multifunctional 2 scanning and imaging photoelectron spectrometer (Japan) equipped with an Al Kα X-ray source. Thermal gravimetric analysis (TGA) was carried out on a TGA Q500 apparatus under a nitrogen atmosphere (flow rate 30 mL min^{-1}) in the temperature range 30−1000 °C (heating rate 10 °C min^{-1}). Scanning electron microscope (SEM) images were obtained on a JEOL 5600LV SEM microscope. High-resolution transmission electron microscope (TEM) images were taken on a JEOL 2010 TEM microscope. SEM and TEM samples were air-dried on silicon wafers and carbon-coated copper grids, respectively, before imaging. Palladium residues left in HCMP networks were analyzed by energy dispersive X-ray (EDX) spectra and elemental analyses. EDX spectra were acquired on the same TEM microscope equipped with an Oxford EDX microanalyzer and operated at the accelerating voltage of 200 kV. Elemental analyses were conducted as follows: a weighed sample was decomposed in aqua regia and then diluted to an accurate volume. Pd content was analyzed on a GBC Avanta Sigma atomic absorption spectrophotometer operating in the Graphite Furnace mode against known standards.

N_2 and CO_2 Adsorption/Desorption Measurements. Nitrogen adsorption/desorption measurements at 77.4 K were performed after degassing the samples under high vacuum at 343 K for at least 20 h using a Quantachrome Quadrasorb SI-MP instrument. CO_2 and N_2 adsorption/desorption isotherms at 273 and 303 K were conducted on a Quantachrome Autosorb-1MP instrument after prior degassing under high vacuum (turbomolecular pump) at 343 K. The specific surface areas were calculated by applying the Brunauer−Emmett−Teller (BET) model to adsorption or desorption branches of the isotherms (N_2 at 77.4 K) using the QuadraWin 5.05 software package. Analysis of the isotherms by commercialized quenched solid density functional theory[56] and grand canonical Monte Carlo[57] methodologies was also done using the QuadraWin 5.05 package.

Ideal Adsorbed Solution Theory (IAST) Calculations. Selectivity was calculated using the common IAST equation: $\alpha = (x_{CO_2}/x_{N_2})/(y_{CO_2}/y_{N_2})$, where α is the selectivity, x the adsorbed amount, and y represents the gas phase composition. The gas phase composition was set 15 vol % CO_2 and 85 vol % N_2, i.e., y_{CO_2} = 0.15 and y_{N_2} = 0.85. The amount adsorbed (x_{CO_2}) was determined following known protocols based on the original IAST method.[58] Basically, the reduced spreading pressures of both adsorbed gases must be equal at equilibrium; this can be calculated numerically. In a first step, the reduced spreading pressures (as a function of total pressure) can be calculated from analytical descriptions of the data of the single-gas adsorption. Those were by obtained using nonlinear regression using either standard Langmuir (N_2 adsorption at 303 K) or dual-site Langmuir models (CO_2 adsorption at 303 K; see Supporting Information for more details and fit parameters). Finally, a Newton−Raphson method implemented within a MatLab (R2011a) script or an octave (open-source software) script can be used to provide the necessary numerical solution, which provides the amount adsorbed (x_{CO_2}) as a function of the total pressure. The adsorbed amount of nitrogen can be calculated as $x_{N_2} = 1 - x_{CO_2}$ as the mixture is a binary one. The used scripts are available for download at http://f-n.hszg.de/fakultaet/hochschullehrerinnen/jens-weber/jens-weber/vermischtesdownloads.html.

Iodine Capture, Release, and Adsorbent Recycle. Iodine uptake experiments based on gravimetric measurements were performed in the following procedure. 10 mg of HCMP powder in an open thermoresistant plastic cap (0.5 mL) and 500 mg of iodine solids were place in a sealed glass vial (7 mL) and heated at 358.15 K and 1.0 bar using an oil bath (Figure S21a). Note that both the iodine solids and caps were placed below the top level of the oil bath. This can dramatically avoid the temperature gradient, which may cause iodine deposition on the surface of polymer powders. After adsorption of the iodine vapor for a while (0−2 h), the adsorbed polymer powders were cooled down to room temperature and weighted. The iodine uptake capacities for HCMPs were calculated by weight gains: $C_u = (W_2 - W_1)/W_1 \times 100$ wt %, where C_u is the iodine uptake capacity and W_1 and W_2 are the mass weight of HCMPs before and after adsorbed iodine vapor. Iodine release in solvents was performed as follows: a 4 mL of quartz cuvette was charged with 1.5 mg of iodine-loaded HCMP powder, and then 3.5 mL of ethanol was added (Figure S21b). Iodine release immediately occurred and was monitored by a UV−vis spectrophotometer within the wavelength range 250−650 nm using the same solvent in the examined solution as a blank. Iodine release and adsorbent recycle upon heating were conducted as follows: 10 mg of iodine-equilibrium **HCMP-3** (C_u: 316 wt %) powder containing 7.6 mg of iodine was charged in an open glass vial (7 mL) and heated at 398.15 K and 1.0 bar in an oil bath. The iodine release efficiency was calculated by weight gains: $E_r = (10 - W_t)/7.6 \times 100$ wt %, where E_r is the iodine release efficiency and W_t is the mass weight of HCMPs after heating release. Recycling percentage (R_p) of the adsorbents was determined as follows: 30 mg of iodine-equilibrium **HCMP-3** (C_u: 316 wt %, 3.16 g g^{-1}) powder was charged in an open glass vial (7 mL) and heated at 398.15 K and 1.0 bar for 45 min in an oil bath (Figure S21c). The recovered **HCMP-3** powder was reused for iodine uptake. The R_p was calculated by weight gains: $R_p = C_u/316 \times 100$ wt %, where R_p is the recycling percentage and C_u is the iodine uptake capacity of **HCMP-3** after heating recovered. A same powder was recycled three times. The above-mentioned iodine uptake, release, and recycling percentage of adsorbents were average values that obtained from three measurements each. To study the changes in conductive property of HCMPs before and after iodine uptake, the resistances (R_{sq}) in ohms/square of one typical polymer, **HCMP-3**, powder as a pellet was measured using a two-point ohmmeter by attaching two lines of copper tap with a same length (0.5 cm) and sequence distance (0.5 cm) onto the surface; the relative error for these measurements is 10%.

■ ASSOCIATED CONTENT

Supporting Information

The Supporting Information is available free of charge on the ACS Publications website at DOI: 10.1021/acs.macromol.6b00901.

Figures S1−S21 and Tables S1−S7 (PDF)

DOI: 10.1021/acs.macromol.6b00901
Macromolecules 2016, 49, 6322−6333

AUTHOR INFORMATION

Corresponding Authors

*E-mail yzliao@dhu.edu.cn (Y.L.).
*E-mail charl.faul@bristol.ac.uk (C.F.J.F.).

Notes

The authors declare no competing financial interest.
All underlying data are provided as Supporting Information accompanying this paper.

ACKNOWLEDGMENTS

We are grateful to the European Commission Marie Curie International Incoming Fellowship (FP7-PEOPLE-2012-IIF TANOGAPPs No. 326385), the Shanghai Pujiang Talent Program (No. 16PJ1400300), the National Natural Science Foundation of China (No. 51673039), and the Fundamental Research Funds for the Central Universities (No. 16D110618) for generous support of this project. This work was also supported by the EPSRC (EP/K502996/1). Mass spectrometric analysis was performed on instrumentation bought through the Core Capability for Chemistry Research−Strategic Investment in Mass Spectrometry EPSRC grant (EP/K03927X/1). The facilities and staff of the Mass Spectrometry service and the NMR service as well as computing resources from the Centre for Computational Chemistry at the University of Bristol are kindly acknowledged.

REFERENCES

(1) Alsbaiee, A.; Smith, B. J.; Xiao, L. L.; Ling, Y. H.; Helbling, D. E.; Dichtel, W. R. Rapid Removal of Organic Micropollutants from Water by a Porous β-Cyclodextrin Polymer. *Nature* **2016**, *529*, 190−194.

(2) (a) Chapman, K. W.; Chupas, P. J.; Nenoff, T. M. Radioactive Iodine Capture in Silver-Containing Mordenites through Nanoscale Silver Iodide Formation. *J. Am. Chem. Soc.* **2010**, *132*, 8897−8899. (b) Katsoulidis, A. P.; He, J. Q.; Kanatzidis, M. G. Functional Monolithic Polymeric Organic Framework Aerogel as Reducing and Hosting Media for Ag Nanoparticles and Application in Capturing of Iodine Vapors. *Chem. Mater.* **2012**, *24*, 1937−1943.

(3) Subrahmanyam, K. S.; Sarma, D.; Malliakas, C. D.; Polychronopoulou, K.; Riley, B. J.; Pierce, D. A.; Chun, J.; Kanatzidis, M. G. Chalcogenide Aerogels as Sorbents for Radioactive Iodine. *Chem. Mater.* **2015**, *27*, 2619−2626.

(4) (a) Zeng, M.-H.; Wang, Q.-X.; Tan, Y.-X.; Hu, S.; Zhao, H.-X.; Long, L.-S.; Kurmoo, M. Rigid Pillars and Double Walls in a Porous Metal-Organic Framework: Single-Crystal to Single-Crystal, Controlled Uptake and Release of Iodine and Electrical Conductivity. *J. Am. Chem. Soc.* **2010**, *132*, 2561−2563. (b) Chapman, K. W.; Sava, D. F.; Halder, G. J.; Chupas, P. J.; Nenoff, T. M. Trapping Guests Within a Nanoporous Metal−Organic Framework Through Pressure-Induced Amorphization. *J. Am. Chem. Soc.* **2011**, *133*, 18583−18585. (c) Yin, Z.; Wang, Q.-X.; Zeng, M.-H. Iodine Release and Recovery, Influence of Polyiodide Anions on Electrical Conductivity and Nonlinear Optical Activity in an Interdigitated and Interpenetrated Bipillared-Bilayer Metal-Organic Framework. *J. Am. Chem. Soc.* **2012**, *134*, 4857−4863.

(5) Vilela, F.; Zhang, K.; Antonietti, M. Conjugated Porous Polymers for Energy Applications. *Energy Environ. Sci.* **2012**, *5*, 7819−7832.

(6) Xu, Y.; Jin, S.; Xu, H.; Nagai, A.; Jiang, D. L. Conjugated Microporous Polymers: Design, Synthesis and Application. *Chem. Soc. Rev.* **2013**, *42*, 8012−8031.

(7) Liao, Y. Z.; Weber, J.; Faul, C. F. J. Conjugated Microporous Polytriphenylamine Networks. *Chem. Commun.* **2014**, *50*, 8002−8005.

(8) Jiang, J.-X.; Su, F. B.; Trewin, A.; Wood, C. D.; Niu, H. J.; Jones, J. T. A.; Khimyak, Y. Z.; Cooper, A. I. Synthetic Control of the Pore Dimension and Surface area in Conjugated Microporous Polymer and Copolymer Networks. *J. Am. Chem. Soc.* **2008**, *130*, 7710−7720.

(9) Wan, S.; Guo, J.; Kim, J.; Ihee, H.; Jiang, D. L. A Belt-Shaped, Blue Luminescent, and Semiconducting Covalent Organic Framework. *Angew. Chem., Int. Ed.* **2008**, *47*, 8826−8830.

(10) Weber, J.; Thomas, A. Toward Stable Interfaces in Conjugated Polymers: Microporous Poly(p-phenylene) and Poly(phenyleneethynylene) Based on a Spirobifluorene Building Block. *J. Am. Chem. Soc.* **2008**, *130*, 6334−6335.

(11) Schmidt, J.; Werner, M.; Thomas, A. Conjugated Microporous Polymer Networks via Yamamoto Polymerization. *Macromolecules* **2009**, *42*, 4426−4429.

(12) Jiang, J.-X.; Laybourn, A.; Clowes, R.; Khimyak, Y. Z.; Bacsa, J.; Higgins, S. J.; Adams, D. J.; Cooper, A. I. High Surface Area Contorted Conjugated Microporous Polymers Based on Spiro-Bipropylenedioxythiophene. *Macromolecules* **2010**, *43*, 7577−7582.

(13) (a) Dawson, R.; Laybourn, A.; Clowes, R.; Khimyak, Y. Z.; Adams, D. J.; Cooper, A. I. Functionalized Conjugated Microporous Polymers. *Macromolecules* **2009**, *42*, 8809−8816. (b) Liao, Y. Z.; Weber, J.; Faul, C. F. J. Fluorescent Microporous Polyimides Based on Perylene and Triazine for Highly CO_2-Selective Carbon Materials. *Macromolecules* **2015**, *48*, 2064−2073.

(14) (a) Weber, J.; Antonietti, M.; Thomas, A. Microporous Networks of High-Performance Polymers: Elastic Deformations and Gas Sorption Properties. *Macromolecules* **2008**, *41*, 2880−2885. (b) Schmidt, J.; Weber, J.; Epping, J. D.; Antonietti, M.; Thomas, A. Microporous Conjugated Poly(thienylene arylene) Networks. *Adv. Mater.* **2009**, *21*, 702−705.

(15) Han, S. S.; Furukawa, H.; Yaghi, O. M.; Goddard, W. A. Covalent Organic Fframeworks as Exceptional Hydrogen Storage Materials. *J. Am. Chem. Soc.* **2008**, *130*, 11580−11581.

(16) Chaikittisilp, W.; Sugawara, A.; Shimojima, A.; Okubo, T. Hybrid Porous Materials with High Surface Area Derived from Bromophenylethenyl-Functionalized Cubic Siloxane-Based Building Units. *Chem. - Eur. J.* **2010**, *16*, 6006−6014.

(17) Lim, H.; Chang, J. Y. Preparation of Clickable Microporous Hydrocarbon Particles Based on Adamantine. *Macromolecules* **2010**, *43*, 6943−6945.

(18) (a) A, S.; Zhang, Y. W.; Li, Z. P.; Xia, H.; Xue, M.; Liu, X. M.; Mu, Y. Highly Efficient and Reversible Iodine Capture Using a Metalloporphyrin-Based Conjugated Microporous Polymer. *Chem. Commun.* **2014**, *50*, 8495−8498.

(19) Chen, Y. F.; Sun, H. X.; Yang, R. X.; Wang, T. T.; Pei, C. J.; Xiang, Z. T.; Zhu, Z. Q.; Liang, W. D.; Li, A.; Deng, W. Q. Synthesis of Conjugated Microporous Polymer Nanotubes with Large Surface Areas as Absorbents for Iodine and CO_2 Uptake. *J. Mater. Chem. A* **2015**, *3*, 87−91.

(20) (a) Lambert, C. Hexaarylbenzenes-Prospects for Toroidal Delocalization of Charge and Energy. *Angew. Chem., Int. Ed.* **2005**, *44*, 7337−7339. (b) Tanaka, Y.; Koike, T.; Akita, M. 2-Dimensional Molecular Wiring Based on Toroidal Delocalization of Hexaarylbenzene. *Chem. Commun.* **2010**, *46*, 4529−4531.

(21) Rosokha, S. V.; Neretin, I. S.; Sun, D. L.; Kochi, J. K. Very Fast Electron Migrations within p-Doped Aromatic Cofacial Arrays Leading to Three-Dimensional (Toroidal) π-Delocalization. *J. Am. Chem. Soc.* **2006**, *128*, 9394−9407.

(22) (a) Short, R.; Carta, M.; Bezzu, C. G.; Fritsch, D.; Kariuki, B. M.; Mckeown, N. B. Hexaphenylbenzene-Based Polymers of Intrinsic Microporosity. *Chem. Commun.* **2011**, *47*, 6822−6824. (b) Carta, M.; Bernardo, P.; Clarizia, G.; Jansen, J. C.; McKeown, N. B. Gas Permeability of Hexaphenylbenzene Based Polymers of Intrinsic Microporosity. *Macromolecules* **2014**, *47*, 8320−8327.

(23) (a) Long, T. M.; Swager, T. M. Minimization of Free Volume: Alignment of Triptycenes in Liquid Crystals and Stretched Polymers. *Adv. Mater.* **2001**, *13*, 601−604. (b) Shen, X. F.; Ho, D. M.; Pascal, R. A. Synthesis and Structure of a Polyphenylene Macrocycle Related to "Cubic Graphite. *Org. Lett.* **2003**, *5*, 369−371.

(24) Mckeown, N. B.; Budd, P. M. Exploitation of Intrinsic Microporosity in Polymer-Based Materials. *Macromolecules* **2010**, *43*, 5163−5176.

DOI: 10.1021/acs.macromol.6b00901
Macromolecules 2016, 49, 6322−6333

(25) Chen, Q.; Luo, M.; Wang, T.; Wang, J. X.; Zhou, D.; Han, Y.; Zhang, C. S.; Yan, C. G.; Han, B. H. Porous Organic Polymers Based on Propeller-like Hexaphenylbenzene Building Units. *Macromolecules* **2011**, *44*, 5573−5577.
(26) Zhang, C.; Peng, L.-H.; Li, B. Y.; Liu, Y.; Zhu, P.-C.; Wang, Z.; Zhan, D.-H.; Tan, B. E.; Yang, X.-L.; Xu, H.-B. Organic Microporous Polymer from a Hexaphenylbenzene Based Triptycene Monomer: Synthesis and Its Gas Storage Properties. *Polym. Chem.* **2013**, *4*, 3663−3666.
(27) Thompson, C. M.; McCandless, G. T.; Wijenayake, S. N.; Alfarawati, O.; Jahangiri, M.; Kokash, A.; Tran, Z.; Smaldone, R. A. Substituent Effects on the Gas Sorption and Selectivity Properties of Hexaphenylbenzene and Hexabenzocoronene Based Porous Polymers. *Macromolecules* **2014**, *47*, 8645−8652.
(28) Shao, Z. C.; Rannou, P.; Sadki, S.; Fey, N.; Lindsay, D. M.; Faul, C. F. J. Delineating Poly(Aniline) Redox Chemistry by Using Tailored Oligo(Aryleneamine)s: Towards Oligo(Aniline)-Based Organic Semiconductors with Tunable Optoelectronic Properties. *Chem. - Eur. J.* **2011**, *17*, 12512−12521.
(29) Pearson, A. J.; Xiao, W. J. Fluorescent Photoinduced Electron Transfer (PET) Sensing Molecules with p-Phenylenediamine as Electron Donor. *J. Org. Chem.* **2003**, *68*, 5361−5368.
(30) Rao, K. V.; Mohapatra, S.; Kulkarni, C.; Maji, T. K.; George, S. J. Extended Phenylene Based Microporous Organic Polymers with Selective Carbon Dioxide Adsorption. *J. Mater. Chem.* **2011**, *21*, 12958−12963.
(31) Jeon, S.-O.; Jeon, Y.-M.; Kim, J.-W.; Lee, C.-W.; Gong, M.-S. Blue Organic Light-Emitting Diode with Improved Color Purity Using 5-Naphthyl-Spiro [Fluorene-7, 9′-Benzofluorene]. *Org. Electron.* **2008**, *9*, 522−532.
(32) Kaplan, S.; Conwell, E. M.; Richter, A. F.; MacDiarmid, A. G. Solid-State Carbon-13 NMR Characterization of Polyanilines. *J. Am. Chem. Soc.* **1988**, *110*, 7647−7651.
(33) Zhang, C.; Liu, Y.; Li, B. Y.; Tan, B. E.; Chen, C.-F.; Xu, H.-B.; Yang, X.-L. Triptycene-Based Microporous Polymers: Synthesis and Their Gas Storage Properties. *ACS Macro Lett.* **2012**, *1*, 190−193.
(34) Jeromenok, J.; Weber, J. Restricted Access: On the Nature of Adsorption/Desorption Hysteresis in Amorphous, Microporous Polymeric Materials. *Langmuir* **2013**, *29*, 12982−12989.
(35) Lozano-Castelló, D.; Cazorla-Amorós, D.; Linares-Solano, A. Usefulness of CO_2 Adsorption at 273 K for the Characterization of Porous Carbons. *Carbon* **2004**, *42*, 1233−1242.
(36) Weber, J.; Du, N. Y.; Guiver, M. D. Influence of Intermolecular Interactions on the Observable Porosity in Intrinsically Microporous Polymers. *Macromolecules* **2011**, *44*, 1763−1767.
(37) Stadie, N. P.; Murialdo, M.; Ahn, C. C.; Fultz, B. Anomalous Isosteric Enthalpy of Adsorption of Methane on Zeolite-Templated Carbon. *J. Am. Chem. Soc.* **2013**, *135*, 990−993.
(38) Yan, Z. J.; Yuan, Y.; Tian, Y. Y.; Zhang, D. M.; Zhu, G. S. Highly Efficient Enrichment of Volatile Iodine by Charged Porous Aromatic Frameworks with Three Sorption Sites. *Angew. Chem., Int. Ed.* **2015**, *54*, 12733−2737.
(39) Falaise, C.; Volkringer, C.; Facqueur, J.; Bousquet, T.; Gasnot, L.; Loiseau, T. Capture of Iodine in Highly Stable Metal−Organic Frameworks: A Systematic Study. *Chem. Commun.* **2013**, *49*, 10320−10322.
(40) Rodriguez, N. M.; Marsh, H. Structure of Coals Studied by Iodine and Water Adsorption. *Fuel* **1987**, *66*, 1727−1732.
(41) Ho, Y. S.; McKay, G. Pseudo-Second Order Model for Sorption Processes. *Process Biochem.* **1999**, *34*, 451−465.
(42) Huang, P.-S.; Kuo, C.-H.; Hsieh, C.-C.; Horng, Y.-C. Selective Capture of Volatile Iodine Using Amorphous Molecular Organic Solids. *Chem. Commun.* **2012**, *48*, 3227−3229.
(43) Mathai, C. J.; Saravanan, S.; Anantharaman, M. R.; Venkitachalam, S.; Jayalekshmi, S. Effect of Iodine Doping on the Bandgap of Plasma Polymerized Aniline Thin Films. *J. Phys. D: Appl. Phys.* **2002**, *35*, 2206−2210.
(44) Hasell, T.; Schmidtmann, M.; Cooper, A. I. Molecular Doping of Porous Organic Cages. *J. Am. Chem. Soc.* **2011**, *133*, 14920−14923.
(45) (a) Xia, Y. N.; Wiesinger, J. M.; MacDiarmid, A. G. Camphorsulfonic Acid Fully Doped Polyaniline Emeraldine Salt: Conformations in Different Solvents Studied by an Ultraviolet/Visible/Near-Infrared Spectroscopic Method. *Chem. Mater.* **1995**, *7*, 443−445. (b) Tigelaar, D. M.; Lee, W.; Bates, K. A.; Saprigin, A.; Prigodin, V. N.; Cao, X. L.; Nafie, L. A.; Platz, M. S.; Epstein, A. J. Role of Solvent and Secondary Doping in Polyaniline Films Doped with Chiral Camphorsulfonic Acid: Preparation of a Chiral Metal. *Chem. Mater.* **2002**, *14*, 1430−1438.
(46) (a) Wang, C. G.; Benz, M. E.; LeGoff, E.; Schindler, J. L.; Allbritton-Thomas, J.; Kannewurf, C. R.; Kanatzidis, M. G. Studies on Conjugated Polymers: Preparation, Spectroscopic, and Charge-Transport Properties of a New Soluble Polythiophene Derivative: Poly(3′,4′-dibutyl-2,2′:5′,2″-terthiophene). *Chem. Mater.* **1994**, *6*, 401−411. (b) Brinkmann, M.; Videva, V. S.; Bieber, A.; André, J. J.; Turek, P.; Humphry-Baker, R. Electronic and Structural Evidences for Charge Transfer and Localization in Iodine-Doped Pentacene. *J. Phys. Chem. A* **2004**, *108*, 8170−8179. (c) Miyajima, N.; Akatsu, T.; Ikoma, T.; Ito, O.; Rand, B.; Tanabe, Y.; Yasuda, E. A Role of Charge-Transfer Complex with Iodine in the Modification of Coal Tar Pitch. *Carbon* **2000**, *38*, 1831−1838.
(47) Morton, J. B.; Preston, K. F. *Magnetic Properties of Free Radicals, Part A: Atom, Inorganic Radicals, and Radicals in Metal Complexes*; Landolt-Bornstein New Series; Springer-Verlag: Berlin, 1977; Vol. *9*, pp 249−250.
(48) Zeng, X.-R.; Ko, T.-M. Structures and Properties of Chemically Reduced Polyanilines. *Polymer* **1998**, *39*, 1187−1195.
(49) Juhola, A. J. Iodine Adsorption and Structure of Activated Carbons. *Carbon* **1975**, *13*, 437−442.
(50) (a) Zwijnenburg, M. A.; Cheng, G.; McDonald, T. O.; Jelfs, K. E.; Jiang, J.-X.; Ren, S. J.; Hasell, T.; Blanc, F.; Cooper, A. I.; Adams, D. J. Shedding Light on Structure-Property Relationships for Conjugated Microporous Polymers: The Importance of Rings and Strain. *Macromolecules* **2013**, *46*, 7696−7704. (b) Slater, A. G.; Cooper, A. I. Function-Led Design of New Porous Materials. *Science* **2015**, *348*, aaa8075−aaa80710.
(51) Frisch, M. J.; Trucks, G. W.; Schlegel, H. B.; et al. *Gaussian 09 (Revision D.01)*; Gaussian, Inc.: Wallingford, CT, 2009.
(52) Yanai, T.; Tew, D. P.; Handy, N. C. A New Hybrid Exchange-Correlation Functional Using the Coulomb-Attenuating Method (CAM-B3LYP). *Chem. Phys. Lett.* **2004**, *393*, 51−57.
(53) (a) Zeng, X. R.; Ko, T. M. Structure-Conductivity Relationships of Iodine-Doped Polyaniline. *J. Polym. Sci., Part B: Polym. Phys.* **1997**, *35*, 1993−2001. (b) Liao, Y. Z.; Strong, V.; Wang, Y.; Li, X. G.; Wang, X.; Kaner, R. B. Oligotriphenylene Nanofiber Sensors for Detection of Nitro-Based Explosives. *Adv. Funct. Mater.* **2012**, *22*, 726−735. (c) Li, X. G.; Liao, Y. Z.; Huang, M. R.; Kaner, R. B. Interfacial Chemical Oxidative Synthesis of Multifunctional Polyfluoranthene. *Chem. Sci.* **2015**, *6*, 2087−2101.
(54) Choi, H. J.; Suh, M. P. Dynamic and Redox Active Pillared Bilayer Open Framework: Single-Crystal-to-Single-Crystal Transformations upon Guest Removal, Guest Exchange, and Framework Oxidation. *J. Am. Chem. Soc.* **2004**, *126*, 15844−15851.
(55) Rathore, R.; Burns, C. L. Preparation of Hexakis(4-Bromophenyl)Benzene (HBB). *Org. Synth.* **2005**, *82*, 30−33.
(56) Ravikovitch, P. I.; Neimark, A. V. Density Functional Theory Model of Adsorption on Amorphous and Microporous Silica Materials. *Langmuir* **2006**, *22*, 11171−11179.
(57) (a) Samios, S.; Stubos, A. K.; Kanellopoulos, N. K.; Cracknell, R. F.; Papadopoulos, G. K.; Nicholson, D. Determination of Micropore Size Distribution from Grand Canonical Monte Carlo Simulations and Experimental CO_2 Isotherm Data. *Langmuir* **1997**, *13*, 2795−2802. (b) Vishnyakov, A.; Ravikovitch, P. I.; Neimark, A. V. Molecular Level Models for CO_2 Sorption in Nanopores. *Langmuir* **1999**, *15*, 8736−8742.
(58) Myers, A. L.; Prausnitz, J. M. Thermodynamics of Mixed-Gas Adsorption. *AIChE J.* **1965**, *11*, 121−127.

DOI: 10.1021/acs.macromol.6b00901
Macromolecules 2016, 49, 6322−6333